A computational tool for determining local dielectric constants in heterogeneous nanoscale systems from molecular dynamics trajectories

Anju Yadav[1], Lela Vuković[1,2,3]*

[1]Department of Chemistry and Biochemistry, The University of Texas at El Paso, El Paso, TX 79968, USA
[2]Computational Science Program, The University of Texas at El Paso, El Paso, TX 79968, USA
[3]Bioinformatics Program, The University of Texas at El Paso, El Paso, TX 79968, USA

**Corresponding Author. E-mail: Lvukovic@utep.edu. Dept. of Chemistry and Biochemistry, UTEP, 500 W. University Ave., El Paso, TX 79968. Phone: 915-747-5701. Fax: 915-747-5748.*

ORCID: Lela Vukovic: 0000-0002-9053-5708

Abstract

In this work, we describe a computational tool designed to determine the local dielectric constants (ε) of charge-neutral heterogeneous systems by analyzing dipole moment fluctuations from molecular dynamics (MD) trajectories. Unlike conventional methods, our tool can calculate dielectric constants for dynamically evolving selections of molecules within a defined region of space, rather than for fixed sets of molecules. We validated our approach by computing the dielectric constants of TIP3P water nanospheres, achieving results consistent with literature values for bulk water. We then applied our tool to more complex systems, the water slabs around solvated phospholipid bilayers, where we observed a lower dielectric constant of water near the bilayer headgroups ($\varepsilon = 20$-50) compared to nanospheres of bulk water ($\varepsilon = 58$-62) with the same number of molecules. Our tool also enabled us to compute the dielectric constants of water in more heterogeneous systems, where water surrounding asymmetrically distributed phospholipids on single-walled carbon nanotubes also exhibited lower dielectric constants than in bulk water nanospheres. Addition of positively charged peptides that bind to phospholipid-nanotube conjugates further lowered the dielectric constants of water in the immediate vicinity of these conjugates. Moreover, we estimated dielectric constants for lipids in symmetric bilayers, where values are well-documented, and for asymmetric phospholipid-wrapped nanotube systems, which were previously unexplored, and found that dielectric constants of phospholipids depend on their arrangement in the assembled aggregate. The results align with literature for bilayers and provide new insights for phospholipid-nanotube systems. The ability of our tool to provide local dielectric constants for both well-studied and novel systems advances our understanding of molecular environments and interactions.

1. Introduction

Interactions among polar and charged functional groups in molecules are crucial for a wide range of biological and engineered molecular processes. These interactions play a key role in protein folding, molecular binding, DNA packaging, and colloidal self-assembly, while also influencing the equilibrium states of nanoscale systems.[1–3] Water, the most common solvent in biological and chemical systems, has a high dielectric constant (labeled as ε or ε_r) of 80, and its presence reduces the electrostatic interactions between charged objects by a factor of 1/80 compared to the interactions in vacuum. When solutes are added into water, the dielectric constant of the solution and electrostatic interactions can change. For example, adding formamide to water increases the dielectric constant of the solution to approximately 100, while adding sugars or alcohols to water decreases the dielectric constant to between 20 and 80, depending on solute concentrations [4] However, these measured dielectric constants reflect the averaged

behavior of the entire solution, including both solute and solvent, and do not account for variations at the molecular scale, where local interactions can differ.

For systems with nanoscale heterogeneity, such as biological macromolecules or synthetic nanomaterials, it can be important to understand the local dielectric environment. Experimental and theoretical studies revealed significant deviations from bulk dielectric properties when polar liquids are confined or near extended surfaces.[5–8] Theories, such as those developed by Kirkwood[9], offer a statistical mechanics-based approach for calculating dielectric constants from molecular dynamics (MD) simulations of heterogeneous systems. This approach typically involves averaging the vector sum of molecular dipole moments over time within a defined region or calculating the static dielectric constant as the zero-frequency component of the power spectrum, calculated from the dipole-dipole correlation function.[10] Previous theoretical work by Yang, et al.[11], building on this approach, introduced the concept of local dielectric constants, which enables separating the contributions of individual components (e.g. solvent versus solute) to the overall dielectric behavior of the system.[11] This work outlined a method to calculate (from MD simulation trajectories) the dielectric constants of individual components by isolating their contributions to the overall dielectric constant. The overall dielectric constant can be derived by combining self-terms, which represent the dielectric response of each component in isolation, and cross-terms among components. The cross-terms were shown to be much smaller than self-terms and can be neglected in calculations.[11]

Several studies have examined the local dielectric constants and their effects in both biological systems and synthetic nanomaterials. For example, in solvated DNA, electrostatic forces influence DNA structure and interactions, where spatially varying dielectric responses influence the stability, conformation, and function of nucleic acids.[10] In nanomaterials, the dielectric environment is often functionally important. For single-walled carbon nanotubes (SWNTs) in different solvents, changes in the dielectric constant of the surrounding solvent can affect SWNT fluorescence. Previous studies have shown that increasing the dielectric constant from 2 to 5 can reduce the SWNT fluorescence emission intensity by more than 50%.[12] This sensitivity of SWNT fluorescence to the dielectric environment is relevant for polymer-wrapped SWNTs solvated in aqueous solutions, which have been shown as excellent optical sensors for bioanalytes of medical importance.[13–20]

Previous work has demonstrated how to calculate the spatially varying dielectric properties from MD simulations, particularly for biomolecules and their aqueous surroundings.[11] Previous research used the established theories to calculate bulk dielectric constants[21–24] or local dielectric constants[10,11,25,26]. However, we did not identify any published codes for performing these local dielectric constant calculations in other heterogeneous nanoscale systems of interest. Here, building on the previously developed methods[11], we developed a computational tool designed to calculate the dielectric constants of subcomponents in charge-neutral inhomogeneous nanoscale systems, based on dipole moment fluctuations from MD trajectories. We demonstrate the application of our tool in several systems, including TIP3P water box, solvated phospholipid bilayers, and lipid-functionalized SWNT systems. Our tool, designed specifically for charge-neutral species, allows determining the local dielectric constants in complex nanoscale systems studied through MD simulations.

2. Methods

In this section, we describe the theoretical framework for calculating local dielectric constants from MD simulations. We also outline the model systems used in the simulations and explain the workflow for calculating the volumes and dielectric constants of the selected molecules within these systems. **Figure 1** illustrates the workflow, using an example of selected molecules for clarity.

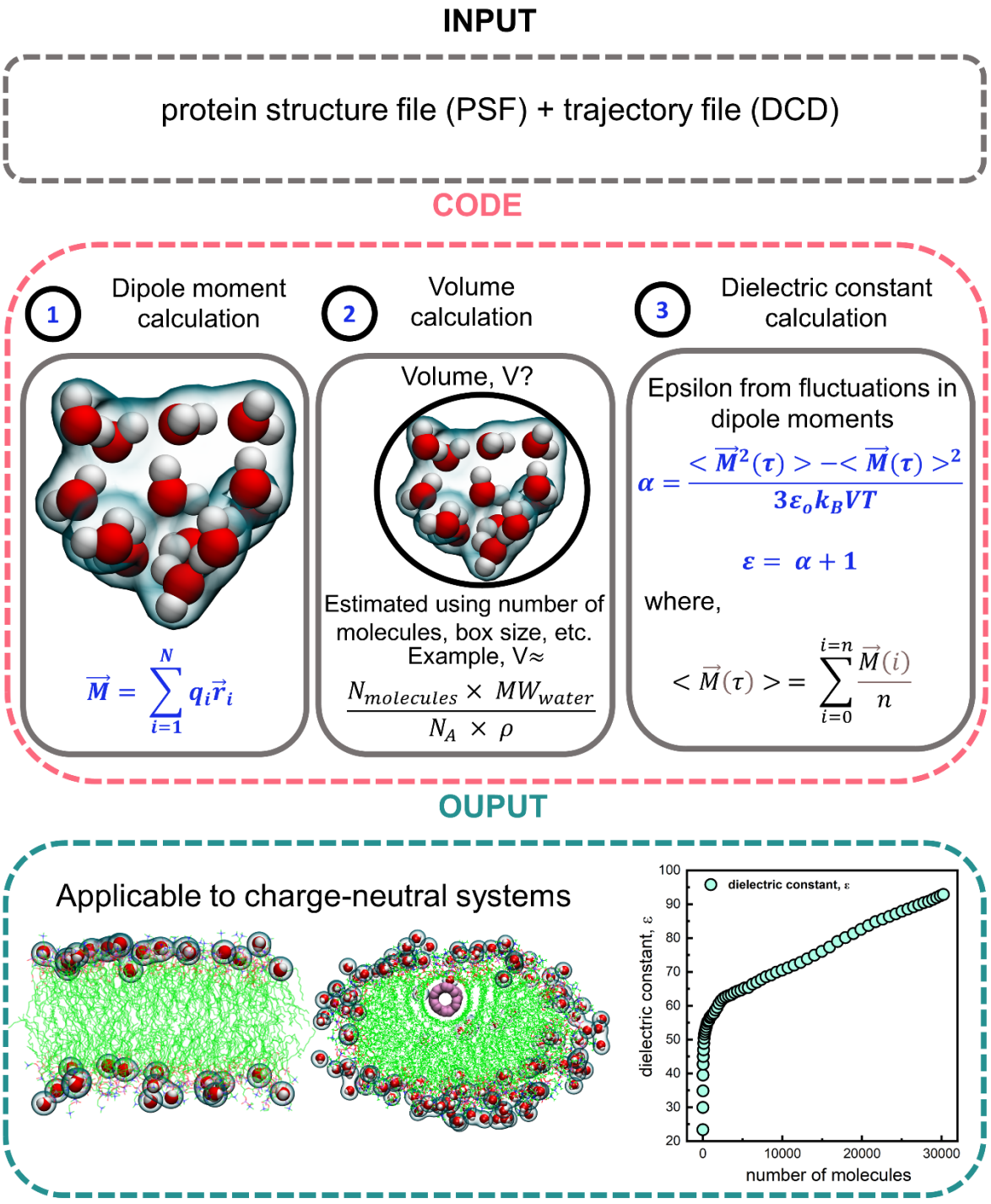

Figure 1. Workflow for computing the dielectric constant for a set of selected molecules from MD simulations.

2.1. Theory Relating Dielectric Constant with Dipole Moment Fluctuations.

Here, we describe the theoretical background used to develop our codes to calculate the dielectric constant of a group of particles examined in MD simulations. The dipole moment of the modelled system consisting of N particles, $\vec{M}$, can be described as:

$$\vec{M} = \sum_{i=1}^{N} q_i \vec{r}_i, \quad \text{Eq. 1}$$

where q_i is the partial charge of the particle *i* as defined in the force field parameters, and $\vec{r}_i$ is the position vector of the same particle. The fluctuations in the dipole moment of a system are directly related to its dielectric constant, ε. Assuming that this system is surrounded by an infinite dielectric medium with the dielectric constant ε_{RF}, the following relationship has been established[11,27–29]:

$$\frac{(\varepsilon-1)(2\varepsilon_{RF}+1)}{(2\varepsilon_{RF}+\varepsilon)} = \frac{<\vec{M}^2>-<\vec{M}>^2}{3\varepsilon_o V k_B T} \equiv \alpha, \qquad \text{Eq. 2}$$

where V is the volume of the system, T is the temperature of the system, and ε_o and k_B are the electric permittivity of vacuum and the Boltzmann constant, respectively. The right-hand side of the equation is defined to be equal to a positive definite quantity named α. When evaluating the fluctuations in the dipole moment ($<\vec{M}^2> - <\vec{M}>^2$), we focus solely on the contribution from the self-terms, neglecting the contribution from the cross-terms due to the latter's negligible magnitude as shown in **Figure S5**.

Two different expressions for ε can be derived from Eq. 1, called ε_1 and ε_2, namely[29]

$$\varepsilon_1 = 1 + \alpha, \text{ if } \varepsilon_{RF} \to \infty \quad \text{Eq. 3}$$

and

$$\frac{(\varepsilon_2-1)(2\varepsilon_2+1)}{2\varepsilon_2} = \alpha, \text{ if } \varepsilon_{RF} = \varepsilon. \quad \text{Eq. 4}$$

As established by Yang, et al.[11], **Eqs. 2** and **3** can be used to determine the dielectric constant of a group of atoms which define a subsystem within a heterogeneous system, based on the fact that evaluation of electrostatic interactions via the Ewald sum in MD simulations (section 2.3 below) sets ε_{RF} at ∞.

2.2. Building Atomistic Models of Simulated Systems.

Here, we built and simulated several systems with increasing levels of heterogeneity, to serve as test cases for calculating dielectric constants of subsystems within them. The systems include a water box, a water-solvated phospholipid bilayer, and a phospholipid-wrapped single walled carbon nanotubes by themselves and interacting with small peptides. The number of molecules and sizes of all the built systems are summarized in **Table S1.**

2.2.1. Water Box. A 100×100×100 $Å^3$ water box consisting of 32054 TIP3P water molecules was constructed using *solvate* plugin in VMD.[30]

2.2.2. POPC Bilayer. A bilayer composed of 1-palmitoyl-2-oleoyl-sn-glycero-3-phosphocholine (POPC) molecules was built using CHARMM-GUI membrane builder[78] with CHARMM36 topology[73]. It was prepared in a tetragonal box, containing a total of 160 POPC molecules (80 per leaflet) and 10720 TIP3P water molecules that were distributed equally over the two leaflets.

2.2.3. POPC-SWNT Systems. A segment of a (6,5) single-walled carbon nanotube, 8 nm in length, was built with the *Carbon Nanostructure Builder* plugin in VMD[30]. The structure of a single POPC molecule was extracted from a POPC membrane segment, built using the *Membrane Builder* plugin in VMD software and the CHARMM36 topology. The systems with mass densities ratios of POPC to SWNT of 9:1 and 15:1 were constructed with POPC arranged cylindrically around the SWNT surface using the procedure described in Ref.[17] All the POPC-SWNT systems were solvated using TIP3P water molecules. The 15:1 POPC-SWNT systems were also simulated when interacting with positively charged membrane-disrupting peptides, colistin (net charge of +5), TAT peptide (net charge of +8) and crotamine-derived peptide (Cro) (net charge of +5). These systems were prepared as described in Ref.[17] with each peptide placed within ~ 5 Å from the SWNT surface (near the thin POPC region). Number of molecules and sizes of the built

systems are described in **Tables S1** and **S2**. Structures of POPC-SWNT conjugates used in constructing these systems were pre-equilibrated in 1 μs-long MD simulations, as described below. POPC-SWNT systems interacting with the membrane-disrupting molecules were solvated in TIP3P water and neutralized in charge by the addition of Cl^- ions, which neutralized the net positive charge created by the presence of Col, TAT or Cro molecules.

2.3. Classical Atomistic Molecular Dynamics Simulations.

All the prepared systems were simulated using the open-source NAMD2.13 package[31] and described with CHARMM36 force field parameters[32–34]. Langevin dynamics equations in the isothermal-isobaric NPT ensemble were used to describe the systems, with temperature and pressure set to 310 K and 1 bar, respectively, and the Langevin coefficient, $\gamma_{Lang,}$ set to 1 ps^{-1}. The integration time step was set to 2 fs, and Coulomb and van der Waals non-bonded interactions were evaluated every one and two time steps, respectively, for all atoms within a 12 Å cutoff distance. The long-range Coulomb interactions were evaluated using the particle-mesh Ewald (PME) method with periodic boundary conditions applied.[35]

One bilayer system was separately simulated using GROMACS 2022.5[36] and CHARMM36 parameters. The Nose-Hoover thermostat[37] and Parrinello-Rahman barostat[38,39] were used to set temperature at 310 K and pressure at 1 bar, respectively. The integration time step was set to 2 fs. The LINCS[40] algorithm was utilized for maintaining bond length constraints, and the PME method was employed to compute the long-range electrostatic interactions accurately.

During the pre-equilibration of bilayer systems, the pressure was controlled by maintaining a constant ratio of the simulation box dimensions in the x-y plane while allowing fluctuations along all three axes. Following pre-equilibration, the systems equilibrated in 50 ns production runs without restraints. In these production runs, the pressure was regulated by keeping the simulation box dimensions constant in the x-y plane while permitting fluctuations along the z-axis.

2.4. Method for Calculating Volumes Occupied by Molecules within Simulated Systems.

The calculations for determining the dielectric constant of selected molecules in the simulated systems require knowledge of the volume these molecules occupy within the simulation box. In this work, the volumes of selected water and lipid molecules need to be calculated.

The volume of selected water molecules in simulated systems was calculated using the established density of TIP3P water at 298.15 K temperature (ρ = 1.002$\pm$ 0.001 g/mL)[41], based on the equation:

$$V_{waters} = \frac{N_{molecules} \times MW_{water}}{N_A \times \rho}, \quad \text{Eq. 5}$$

where $N_{molecules}$ correspond to the number of water molecules in the selection, MW_{water} is the molecular mass of one water molecule, and N_A is Avogadro's constant. The volumes obtained for various spherical selections are summarized in **Table S3**. The volumes were calculated by averaging over last 20 % of (fluctuations in dipole moment) frames of the trajectory.

The volume of lipid molecules ($V_{lipids\ (bilayer)}$) in the bilayer system was calculated using the following equation:

$$V_{lipids\ (bilayer)} = V_{unit-cell} - V_{waters}, \quad \text{Eq. 6}$$

where, $V_{unit-cell}$ is the volume of the simulated unit cell and can be calculated as the product of the lengths of the unit cell in x, y, and z directions. The volumes of local selections of lipids were approximated based on the number of molecules as summarized in **Table S4**. The volumes were calculated by averaging over last 20 % of frames of the trajectory.

For POPC-SWNT systems, the volume of lipid molecules was calculated as follows,

$$V_{lipids\ (POPC-SWNT)} = V_{box} - V_{water} - V_{SWNT}, \quad \text{Eq. 7}$$

where, V_{SWNT} was calculated as $V_{SWNT} = \pi \times r^2 \times h$, where r and h are the effective radius and the length of the SWNT, respectively. The effective radius of the SWNT is estimated as $r = r' + r_{vdW}$, where r' is the radius of the SWNT and r_{vdW} is the vdW radius of carbon atoms constituting the SWNT. The values used in the calculations were r' = 0.38 nm, r_{vdW} = 0.099 nm, and, h = 8.01 nm, respectively, obtained by averaging in MD trajectories. The average volumes of various local selections of lipids in control 9:1 POPC-SWNT system are reported in **Table S5**. The volumes of other POPC-SWNT systems were calculated similarly. All the volume calculations described above were performed using python and tcl scripts.

2.5. Calculation of Dielectric Constants of Selections of Molecules within Simulated Systems.

The dielectric constant of a selection of molecules in our simulated systems was calculated using the expression that combines **Eqs. 1** and **2**, namely:

$$\varepsilon = \frac{<\vec{M}^2(\tau)> - <\vec{M}(\tau)>^2}{3\varepsilon_o k_B V T} + 1, \quad \text{Eq. 8}$$

where the expression $<\vec{M}^2(\tau)> - <\vec{M}(\tau)>^2$ corresponds to the time correlation function of the fluctuations in the dipole moment $\vec{M}(\tau)$ of the selected atoms, averaged over the ensemble of particles in the selection (i.e. all the atoms in the selection), and τ is the time interval for which the dipole moment is being calculated. For instance, at any time frame n in the trajectory, $<\vec{M}(\tau)>$ is an average over the time interval τ, where τ = n and i represents a series of all the previous time frames:

$$<\vec{M}(\tau)> = \sum_{i=0}^{i=n} \frac{\vec{M}(i)}{n}. \quad \text{Eq. 9}$$

Fluctuations in the dipole moment $\vec{M}(\tau)$ were calculated using the tcl scripts and the calculations of the dielectric constant ε were performed using a bash script. The fluctuations in dipole moment were calculated by averaging over last 20% of frames of the trajectory.

Our script calculates epsilon (dielectric constant, ε) based on Eq. 8 using the fluctuations in the dipole moment for a given selection of atoms in the input PSF and DCD files as shown in described in **Figure 2**.

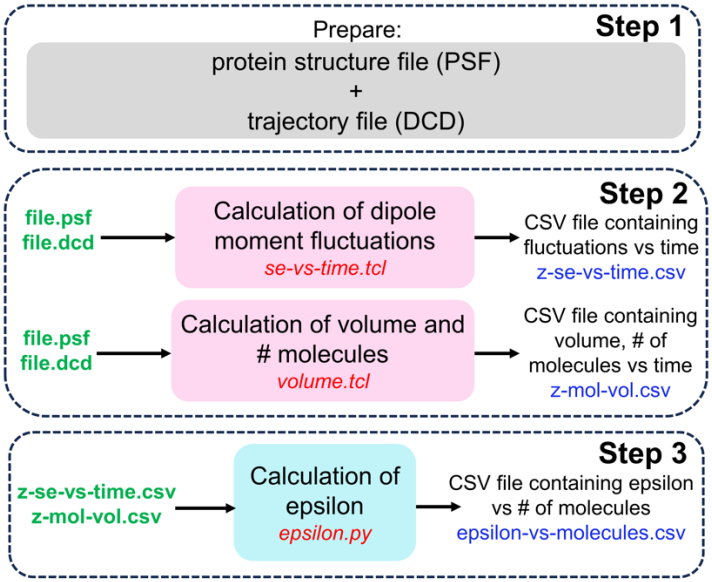

Figure 2. Steps for using our scripts to calculate the dielectric constants of the selected subsystem from MD trajectories.

2.6 Steps in Using *tcl* and python Scripts.

The steps for using our tcl and python scripts are summarized in **Figure 2**. Our *tcl* scripts (provided at https://github.com/vukoviclab/LocalDielectricMD) can be used for any charge-neutral system for which the input PSF and DCD MD trajectory files are available, which need to be specified in two scripts se-vs-time.tcl and volume.tcl. Next, the selections of groups or molecules for which the dielectric constant is to be calculated should be provided. As the scripts used to calculate the fluctuations in the dipole moment and volumes are based on *tcl* language in VMD, the selection should match the names in the PSF file and should be compatible with the *atomselect* command in VMD. The output of the *tcl* scripts includes the following CSV files: z-se-vs-time.csv and z-mol-vol.csv. Next, we give an example for calculation of dielectric constants for water selections. A python script epsilon.py should be provided the paths to z-se-vs-time.csv and z-mol-vol.csv files, in order to output the plot of the number of molecules in the selections and the calculated dielectric constants for those selections. For calculating the volume of selections, we provide a script that is based on the number of molecules to obtain the volume of selections as described in Methods. Users can use custom scripts to obtain volumes of their selected molecules depending on the type of system.

3. Results and Discussion

3.1. Application of Our Scripts to Calculate Local Dielectric Constants in Model System 1: Water Nanospheres.

To demonstrate the capabilities of our scripts and compare its results to literature values, we applied it to a model system of water nanospheres of varying radii, selected from a cubic box of water containing 32,054 TIP3P water molecules, as shown in **Figure 3a**. We first calculated the fluctuations in the dipole moment, $< \vec{M}^2(\tau) > - < \vec{M}(\tau) >^2$, plotted in **Figure 3b** for whole water box system and a nanosphere with radius of 1 nm. For both cases, the fluctuations in the dipole moment converge over the time of 50 ns. After the convergence was confirmed, the script was used to calculate the local dielectric constant ε for selected water nanospheres with varying radii, from r = 0.2 to r = 8.5 nm, as shown in **Figure 3c**. The nanospheres with r = 1, 2 and 5 nm, containing 158, 1194, and 17889, water molecules, were found to have $\varepsilon = 50.73$, 57.38, and 80.10, respectively.

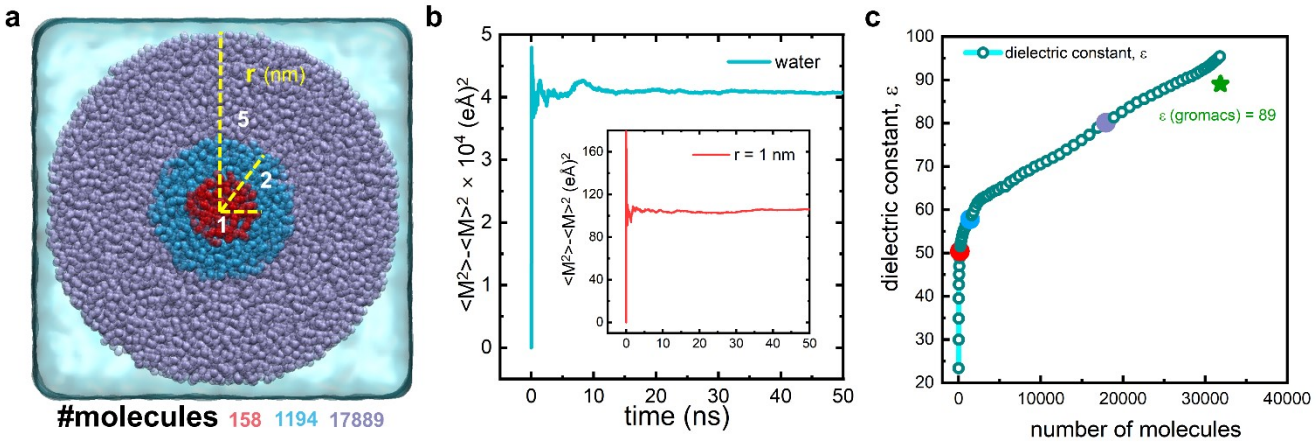

Figure 3. Dielectric constants of water nanospheres. (a) A snapshot of the simulated water box containing 32,054 TIP3P water molecules. The water nanosphere selections with r = 1, 2, and 5 nm are shown in red, blue, and violet. (b) Fluctuations in dipole moment for all the water molecules in the box. (inset) The fluctuations in the dipole moment for the water molecules in the nanosphere with 1 nm radius. (c) Dielectric constant for water nanospheres as a

function of the number of molecules in the nanospheres. The dielectric constants of water nanosphere selections with r = 1 nm, 2 nm, and 5 nm are shown as red, blue, and violet points.

As the number of molecules in the selection increases further to include the whole cubic box, the dielectric constant increases and eventually converges to a value of $\varepsilon = 92.65 \pm 1.30$ The dielectric constant profiles were shown to be reproducible (**Figure S1**). The obtained result is in reasonable agreement with the known value of ε for liquid water ($\varepsilon \approx 80$), the reported dielectric constant of the TIP3P water model ($\varepsilon = 92 \pm 5$ at 298 K), and the value of $\varepsilon = 89$ obtained using Gromacs *gmx dipole* code. The convergence of the results and the value obtained for the whole simulated box demonstrate the accuracy and effectiveness of our code in calculating local dielectric constants in molecular systems.

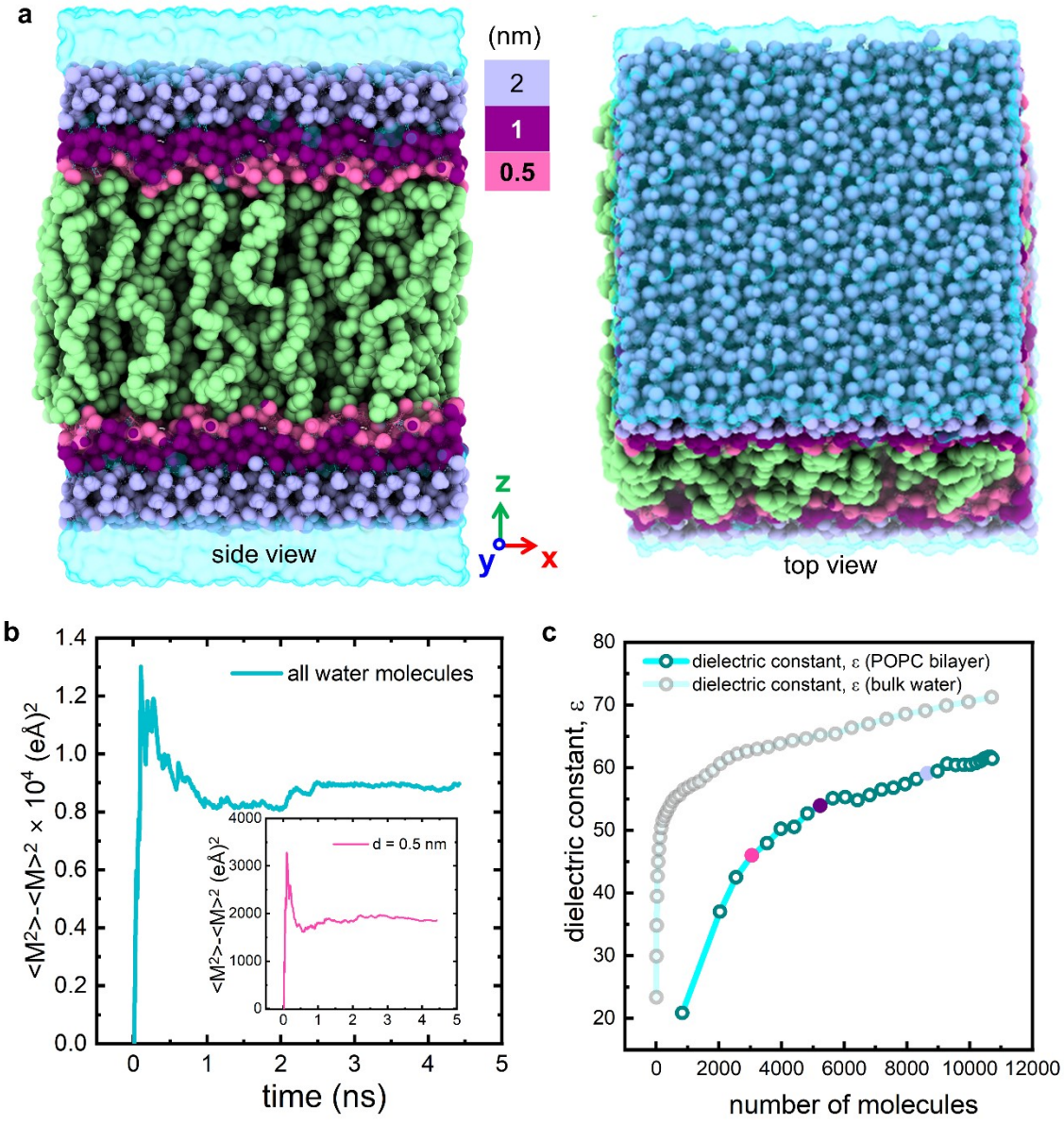

Figure 4. Dielectric constants of water slabs in lipid bilayer system. (a) Snapshot of solvated bilayer system containing 160 POPC lipids and 10720 water molecules. The local selections of water molecules in slabs with variable thickness are highlighted in pink, purple and violet colors. POPC lipids are shown in light green, and the water solvent (other than the slab selections) is shown as a light blue surface. (b) Fluctuations in dipole moment for all the water molecules in the simulation box shown. (inset) Fluctuations in the dipole moments for the water molecules in the slab with thickness of d =0.5 nm. (c) Dielectric constant for water slabs of varying thickness, starting with d = 0.2 nm to r

= 3.2 nm as a function of the number of molecules in the slab. The dielectric constants of water slab selections with d = 0.5 nm, 1 nm, and 2 nm are shown as pink, purple, and violet points. The transparent gray curve shows dielectric constant for the same number of molecules in water nanospheres.

3.2. Application of Our Scripts to Calculate Local Dielectric Constants in Lipid-Based Model Systems: Water Slabs Surrounding a POPC Bilayer and Water Shells Around POPC-Wrapped Nanotubes.

In MD simulations of heterogeneous systems, it can be critical to determine the local dielectric constant for different phases composed of various molecules. One such system of importance, both biologically and for bioengineering applications, is the lipid bilayer solvated in water, which serves as a simple model for biological cell membranes. The dielectric constant of the solvent surrounding the lipids in a bilayer is directly related to the solubility and permeability of lipid membranes,[42] making it a key parameter for understanding membrane behavior.

We examined the performance of our scripts on a model lipid bilayer solvated in water, shown in **Figure 4a**. We calculated the dielectric constants of thin water slabs surrounding the lipid bilayer headgroups, accounting for the fact that the local environment is now better represented by a slab geometry rather than the nanosphere geometry used in our previous example. The dielectric constant was calculated as a function of the thickness of the water slabs (d), with representative cases of 0.5 nm, 1 nm, and 2 nm highlighted in **Figure 4a**. First, we examined the dipole moment fluctuations of all water molecules in the system, as well as those forming the thinnest slab (d = 0.5 nm). **Figure 4b** shows that dipole moment fluctuations converged after 5 ns for both cases.

Next, we calculated the dielectric constants for water slabs of varying thickness (d = 0.2 nm to d = 3.2 nm), as shown in **Figure 4c**. Thin slabs that are near the bilayer headgroup region have dielectric constants in the range of 20 – 50, lower than that of water nanospheres containing a similar number of water molecules, which had a dielectric constant of 58 - 62. This reduction in the dielectric constant could be due to the presence of zwitterionic groups near the water molecules, which restrict water orientations and reduce their fluctuations, or to water molecules occupying spaces near the lipids hydrophobic tails. For thicker slabs (d > 2 nm), which include water molecules both near and further from the lipids, the dielectric constant increases ($\varepsilon \sim 62$), but remains lower than that of bulk water. The results obtained for all the water in our system are in agreement with reported dielectric constants for similar bilayer systems where ε varies between 20 – 60, [42–46] demonstrating the applicability of our scripts for heterogeneous systems. It is important to note that, unlike commonly used tools such as GROMACS' *gmx dipole*, which report dielectric constants for entire systems, our code can calculate the dielectric constants of local regions (e.g., slabs).

Next, we examined a related POPC-based system, specifically POPC-coated SWNTs. The local dielectric constant has been identified as a key factor influencing the fluorescence emission by SWNTs.[47,48] Understanding how the local dielectric constant around SWNTs is affected by binding of analytes could provide mechanistic understanding of optical detection of bioanalytes by SWNTs. Many SWNT-based sensors are coated with polymers such as surfactants, lipids, single-stranded DNA and RNA, peptides, and other molecules.[49–54] This study calculates the local dielectric constants around POPC-coated SWNTs, which were shown to be useful for detecting membrane-perturbing molecules.[17,55]

One of the examined POPC-SWNT systems is shown in **Figure 5a.** It consists of an 8 nm long SWNT wrapped by POPC lipids, with 9:1 POPC:SWNT mass density ratio. Another system, not shown here but examined in Ref.[17] contains the same SWNT segment coated by POPC with 15:1 POPC:SWNT mass density ratio. Due to the periodic boundary conditions in the simulations, this setup effectively represents an infinitely long POPC-coated SWNT. To determine the dielectric constant of the water surrounding the POPC and SWNT, we first selected water molecules within thin cylindrical shell-like volumes of varying thickness around the POPC-SWNT conjugates (**Figure 5a**). The water molecules in the 1 nm-thick

cylindrical shell represent the immediate local environment of the conjugate. The convergence of the fluctuations in dipole moment for the water molecules in both systems was verified (for 9:1 and 15:1 POPC:SWNT mass density ratios, **Figure S2**). Due to conformational changes in the system, where the initial symmetric arrangement of POPC around the SWNT transitions to a more asymmetric configuration, the fluctuations in dipole moment stabilize after approximately 200 to 500 ns. Next, we calculated the dielectric constants for cylindrical water shells of varying thicknesses, ranging from 0.2 nm to 7 nm. The dielectric constant profiles for both POPC-SWNT systems, shown in **Figures 5b-c,** display a similar trend as observed for water molecules in the pure bilayer system: an initial rapid increase in dielectric constant, followed by a slower rise.

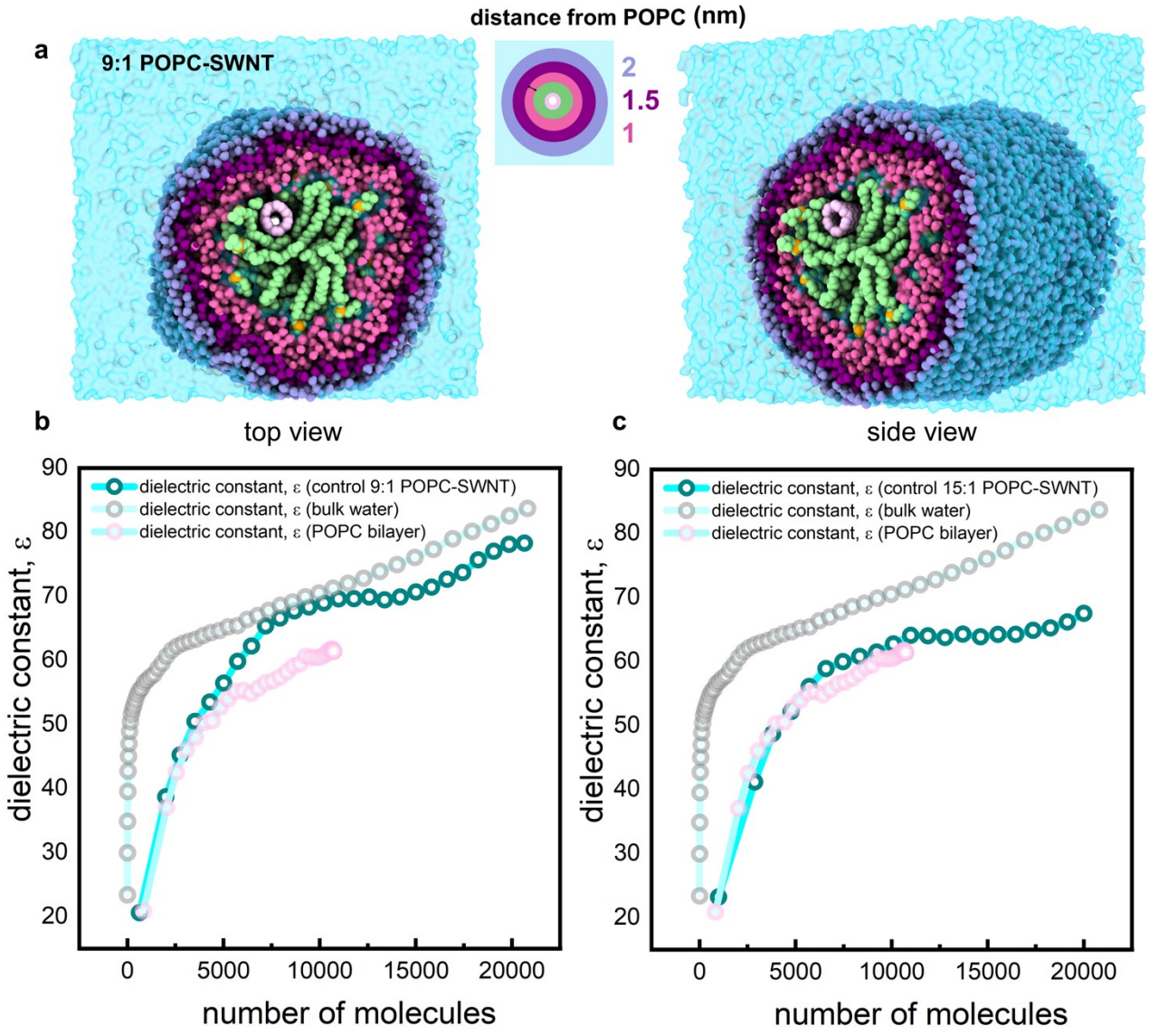

Figure 5. Dielectric constant of cylindrical or ellipsoidal shells of water in POPC-SWNT systems. (a) Snapshots of top and side views of 9:1 POPC-SWNT system. The local selections of water molecules in cylindrical shells with variable thickness are highlighted in pink, purple and violet. POPC atoms are shown in light green (C), red (O), blue (N) and orange (P), and water is shown as a light blue surface. (b) Dielectric constant for water cylindrical shells of varying thickness, ranging from 0.2 nm to 7 nm for the 9:1 POPC-SWNT system. (c) Dielectric constant for water ellipsoid shells of varying thickness, ranging from 0.2 nm to 7 nm for the 15:1 POPC-SWNT system. The transparent gray curves in (b,c) depict the dielectric constant for the same number of molecules in water nanospheres, and the transparent pink curves depict the dielectric constant of the same number of water molecules in water slabs around the POPC bilayer.

The performed calculations allow us to compare the effect of water environment on the dielectric constant. For example, bulk-like water nanospheres of ~ 2,400 water molecules have dielectric constant of ~ 60, whereas the slab and shell selections in bilayers and 9:1 POPC-SWNTs with the same number of water molecules have dielectric constants of 37-38. These results indicate strong effects that POPC surroundings have on fluctuations in dipole moments of water molecules and the local dielectric constants. The results also show that the percentage of water molecules in direct contact with POPC is smaller in the 9:1 POPC:SWNT system compared to the 15:1 POPC:SWNT system (for the same selection criterion), due to differences in cylindrical water shell geometry (in the 9:1 system) and the elliptical water shell geometry (in the 15:1 system), with its high eccentricity (**Table S6**). The percentage of water molecules in direct contact with the POPC lipids is 39% in the 9:1 POPC-SWNT system, compared to 43% in the 15:1 system. This increase in water-lipid interactions due to the larger percentage of non-bulk-like water molecules may explain the lower dielectric constant observed in the 15:1 POPC-SWNT system. Our scripts also allow us to determine the effects that proximity to head groups versus the proximity to hydrophobic tails has on the dielectric constants of local water (**Table S7**). Finally, as the cylindrical shells increase in thickness, their dielectric constants increase towards values observed for more bulk-like water (~88 for the 9:1 POPC-SWNT system and ~78 for the 15:1 system).

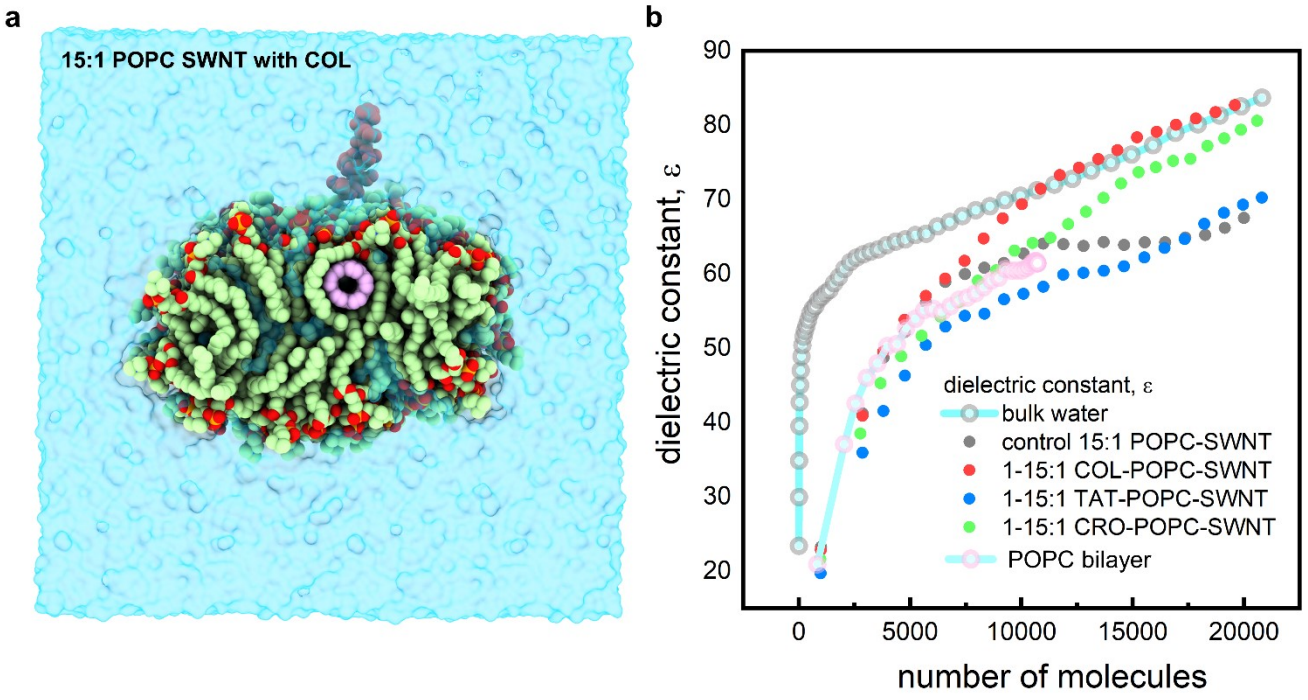

Figure 6. Dielectric constant profiles for water in POPC-SWNT systems containing antimicrobial peptides. (a) Snapshots of 15:1 POPC SWNT system containing one colistin molecule. Col molecule is shown in red as van der Waals spheres (protruding from the corona). POPC atoms are shown in light green (C), red (O), blue (N), and orange (P). Solvent is shown in light blue color as surface representation. SWNT is shown in pink color. (b) Epsilon for various local selections starting with molecules within 0.2 nm of POPC molecules for 15:1 POPC-SWNT system containing the added single peptides near the SWNT surface. The dielectric constant profile for water nanospheres and water slabs around POPC bilayer are shown as transparent gray circles and transparent pink circles.

One interesting question is how the addition of compounds that disrupt the POPC corona on SWNT affects the dielectric constants of the local water layers surrounding the SWNT and POPC. Previous studies have shown that perturbation of the POPC corona by such compounds can be detected through changes in the

fluorescence emission of SWNTs.[17,55] We investigated the local dielectric constants of water around POPC-SWNTs for systems with 15:1 POPC mass density ratios, where the POPC coronas were disrupted by three antimicrobial peptides: a TAT-derived peptide, colistin, and a crotamine-derived peptide. A representative POPC-SWNT system with one Col disruptor is shown in **Figure 6a**, while the other systems are discussed and analyzed in Ref. [17].

In all systems, convergence in dipole moment fluctuations of two representative water selections was confirmed (**Figure S3**), however, this convergence occurred after between 200 and 700 ns due to large changes in binding especially during the first few hundred nanoseconds, when the molecules diffuse from the solvent towards POPC corona and bind there. In all cases, the water nearest the POPC-SWNT (in the thinnest layers, containing fewer than 500 water molecules) exhibited a lower dielectric constant than pure water. The presence of peptides additionally lowers the dielectric constant of water molecules in the immediate surroundings of POPC (e.g. selections of ~2,700 water molecules) for all three peptides (**Figure 6b**), and mostly for TAT, the peptide with the highest net charge (+8).

3.3. Application of Our Code to Calculate Local Dielectric Constants of Lipid Selections in POPC Bilayers and POPC-wrapped Nanotubes.

The dielectric constant of lipids within a biological membrane bilayer is crucial for determining membrane permeability to ions, the membrane's response to externally applied potentials, and the interfacial properties between the membrane and its surrounding solvent.[56,57] Several studies have examined the dielectric constant of bilayers composed of various lipid types.[58–65] Using our custom code, we calculated the dielectric constants for a bilayer consisting of 160 POPC lipids, individual lipids within the bilayer, 80 headgroups (from one layer), and 80 tails (from one layer), as depicted in **Figure 4a**. The fluctuations in the dipole moments for lipid components converged only after ~ 500 ns of simulation (**Figure S4).**

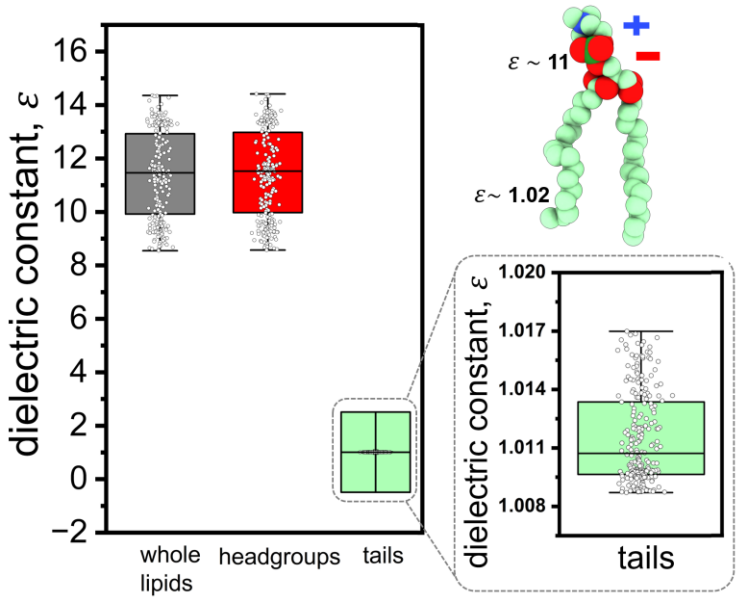

Figure 7. Dielectric constant of lipids in a solvated bilayer system. Dielectric constants of all POPC molecules in a bilayer (160), all the POPC headgroups, and all the POPC hydrophobic tails. The inset plot is the expanded representation of the values obtained for the POPC hydrophobic tails. The dielectric constant was calculated for all the lipids or headgroups or tails in the bilayer system over time, and white circles represent the range of dielectric constant for the selections over time.

The calculated dielectric constants, shown in **Figure 7**, indicate that for all lipid molecules, dielectric constant averages at ~11 for all the lipids in the system and fluctuates between 8 and 14 over the converged time frames, as the lipid molecules undergo conformational changes. Additionally, the dielectric

constant of the POPC hydrophobic tails from all lipids in the system averages around 1.02, while that of the polar POPC headgroups from all lipids in the system is approximately 11. These results are consistent with reported values in the literature, where dielectric constants typically range from 1 to 3 for the hydrophobic region of lipid membranes and from 7 to 15 for the polar zwitterionic headgroup region[66–68].

Furthermore, we compared the dielectric constants obtained with our code with those computed with the *gmx dipole* function. The comparison, summarized in **Table S8**, shows discrepancies due to differences in how volumes are defined. The *gmx dipole* function appears to base its calculations on the volume of the entire simulation unit cell rather than the volume of the local selection (**Table S8**), whereas our code bases the calculations on the volume of the local selection. As a result, the dielectric constant values from our code are not directly comparable to those obtained using the *gmx dipole* function.

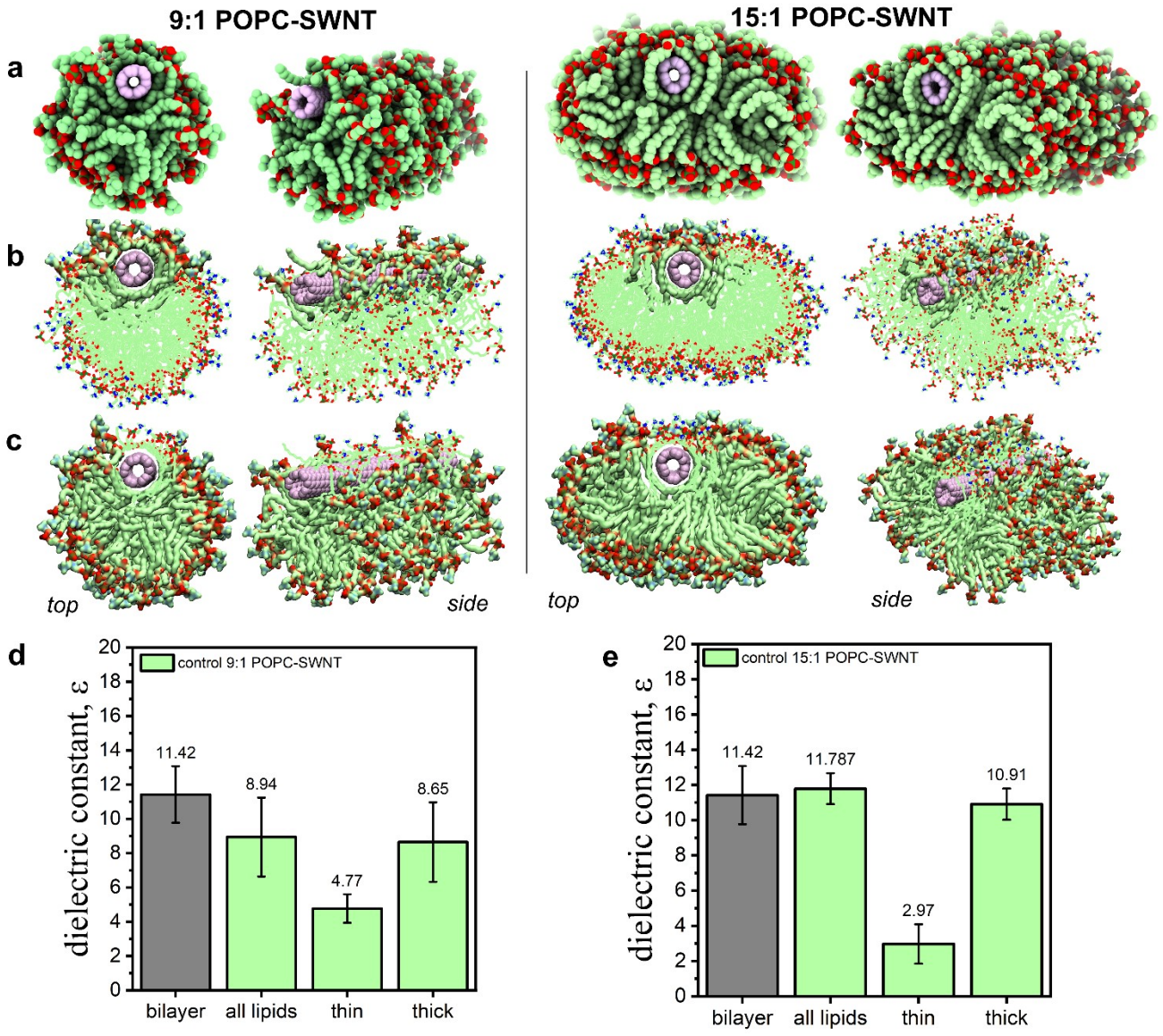

Figure 8. Dielectric constant of lipids in control POPC-SWNT systems. (a) Snapshots of top and side views of 9:1 and 15:1 POPC SWNTs. (b) Snapshots of POPC lipids defined as forming the thin regions of the corona around SWNTs (shown as van der Waals spheres, whereas the remaining the POPC molecules are shown as lines). (c) Snapshots of POPC lipids defined as forming the thick regions of the corona around SWNTs (shown as in panel b). (d) Dielectric constants of various local POPC selections around SWNT for 9:1 POPC-SWNT system. (e) Dielectric

constants of various local POPC selections around SWNT for 9:1 POPC-SWNT system. The color scheme is the same as in the above figures. The dielectric constant of lipids in pure bilayer systems is shown as a gray bar.

With the ability to compute dielectric constants for lipid selections, we applied our code to examine how the dielectric constant of the POPC corona around SWNTs, where the POPC molecules are asymmetrically distributed, differs from that of the POPC bilayer. Snapshots of the 9:1 and 15:1 POPC-SWNT systems are shown in **Figure 8a**. The dielectric constant obtained for all lipids in the 15:1 POPC-SWNT system is 11.79, which is higher than that of the 9:1 POPC-SWNT system, found to be 8.94 (**Figure 8d,e**). Given the asymmetry of the POPC corona, we further examined the dielectric constants in the thin and thick regions of the corona (**Figure 8b,c**). The dielectric constants of the lipids in the thin regions of both the 9:1 and 15:1 systems are lower than those in the thick regions. The lipids in the thick region, especially in the 15:1 system, resemble the bilayer arrangement, exhibiting dielectric constants closer to those of a pure bilayer and higher than those in the thin region. These results illustrate how the aggregate shape can influence the dielectric constants of lipid assemblies.

Conclusion

In this work we implemented a previously established method and developed a computational tool to determine the dielectric constant of subcomponents of charge-neutral heterogeneous systems, based on dipole moment fluctuations measured in molecular dynamics trajectories. We first validated our computational approach by evaluating the dielectric constant of TIP3P water nanospheres with varying radii and confirmed agreement with literature values for large nanospheres (bulk water regime) [69]. Notably, our code has the capability to calculate the dielectric constant of dynamically changing selections of molecules within a specified region of space. For instance, in the case of a nanosphere with a 1 nm diameter, specific water molecules can enter and leave the defined space. Unlike methods such as *gmx dipole*, our code does not calculate the dielectric constant for a fixed set of molecules by index. Instead, it computes the dielectric constant for water molecules occupying the defined space at any given time. Also, our code assumes that volume of the sub-selections will be calculated by the user, rather than using the volume of the whole unit cell for calculations.

Next, we applied our tool to more heterogeneous systems, calculating the dielectric constants for slabs of water molecules of varying thicknesses around solvated bilayers. The water molecules located in thin slabs of ~2,400 molecules nearest to the bilayer headgroup region exhibited dielectric constants of ~37-38, which is lower than the value of ~60 found for nanospheres of bulk water with the same number of molecules. This reduction in dielectric constant near the bilayer system was likely due to the presence of zwitterionic groups surrounding the water molecules, which constrain their orientations and reduce their fluctuations. (**Table S7).** In a 0.5 nm thick slab, 50% of the water molecules are directly interacting with the zwitterionic headgroups, which have a dielectric constant of 30.7, whereas only 5% of the water molecules are in contact with the hydrophobic tails, characterized by a dielectric constant of 23.8. In thicker water slabs surrounding the lipids (3 nm wide), where more water molecules have bulk-like behavior, the dielectric constant increases to 62. The dielectric constants calculated for water in the bilayer system are consistent with reported values for similar systems in the literature[42–46].

To examine how the dielectric constant of water is affected by increased degrees of heterogeneity in related systems, we tested our code for water surrounding SWNTs covered by POPC coronas[17,55]. Water molecules in cylindrical shells of different thickness around the POPC lipids had significantly smaller dielectric constants than bulk water nanospheres containing the same number of molecules. Addition of positively charged peptide disruptors of POPC assemblies further lowered the dielectric constants of waters in the immediate vicinity of POPC and SWNTs.

Next, we evaluated the performance of our code in estimating the dielectric constants of more complex molecules, specifically lipids, in both symmetric arrangements (bilayers) and asymmetric arrangements (POPC-wrapped SWNTs). Using our code, we found that the dielectric constants of lipid molecules in bilayers are approximately 11, and the contributions from the hydrophobic tails of the lipid molecules average around 1.02, while the contribution from the polar headgroups is approximately 11. These calculated values correlate well with existing literature, which reports dielectric constants for the hydrophobic region of lipid membranes typically ranging from 1 to 3 and for the polar zwitterionic headgroup region from 7 to 15 [66–68]. In systems where the orientation and arrangement of lipids in the corona structures differ notably from those in a pure bilayer, we calculated dielectric constants of 9 for POPC lipids in the 9:1 POPC-SWNT system and 11.8 in the more bilayer-like 15:1 POPC-SWNT system, indicating that geometry of the self-assembled aggregate also influences its dielectric constant.

In summary, our computational tool successfully estimates the dielectric constants of various subcomponents within neutral, heterogeneous systems, as demonstrated in this study. The tool accurately reproduces dielectric constant values observed in literature-reported systems (pure water, bilayers) and can calculate dielectric constants in new systems and subsystems. Although it is currently designed for neutral species and systems, our tool has the potential to be extended for use with charged systems.

Supporting Information. Reproducibility of dielectric constant profiles of water molecules in water box (bulk water) in two independent runs; Fluctuations in dipole moment of water molecules in control POPC-SWNT systems; Fluctuations in dipole moment of water molecules in POPC-SWNT systems bound to antimicrobial disruptors; Fluctuations in dipole moment of various lipid selections; Summary of the simulated POPC-SWNT and bilayer systems; Summary and composition of the POPC-SWNT systems with single disruptor molecules binding to the thinnest part of the POPC corona; Volumes of waters for different local spherical selections; Volumes of lipids for different local lipid selections in pure bilayer system; Volumes of lipids for different local lipid selections in control 9:1 POPC-SWNT system; Percentage of number of water molecules in direct contact of POPC in POPC bilayer, control 9:1 POPC-SWNT, control 15:1 POPC-SWNT systems; Comparison of number of water molecules near the headgroup and tails of POPC in POPC bilayer, control 9:1 POPC-SWNT, control 15:1 POPC-SWNT systems; Comparison of dielectric constants obtained using our code and GROMACS (*gmx dipole*)

Acknowledgements

We acknowledge the support by the NSF CBET-2106587 award and the computer time provided by the Texas Advanced Computing Center (TACC).

References

(1) Israelachvili, J.; Wennerström, H. Role of Hydration and Water Structure in Biological and Colloidal Interactions. *Nature* **1996**, *379* (6562), 219–225. https://doi.org/10.1038/379219a0.

(2) Zhou, H.-X.; Pang, X. Electrostatic Interactions in Protein Structure, Folding, Binding, and Condensation. *Chem Rev* **2018**, *118* (4), 1691–1741. https://doi.org/10.1021/acs.chemrev.7b00305.

(3) Yan Levin. Electrostatic Correlations: From Plasma to Biology. *Reports on Progress in Physics* **2002**, *65* (11), 1577. https://doi.org/10.1088/0034-4885/65/11/201.

(4) Akerlof, G. DIELECTRIC CONSTANTS OF SOME ORGANIC SOLVENT-WATER MIXTURES AT VARIOUS TEMPERATURES. *J Am Chem Soc* **1932**, *54* (11), 4125–4139. https://doi.org/10.1021/ja01350a001.

(5) Schaaf, C.; Gekle, S. Spatially Resolved Dielectric Constant of Confined Water and Its Connection to the Non-Local Nature of Bulk Water. *Journal of Chemical Physics* **2016**, *145* (8). https://doi.org/10.1063/1.4960775.

(6) Mukherjee, S.; Mondal, S.; Bagchi, B. Distinguishing Dynamical Features of Water inside Protein Hydration Layer: Distribution Reveals What Is Hidden behind the Average. *J Chem Phys* **2017**, *147* (2), 024901. https://doi.org/10.1063/1.4990693.

(7) Jiménez-Ángeles, F.; Harmon, K. J.; Nguyen, T. D.; Fenter, P.; Olvera de la Cruz, M. Nonreciprocal Interactions Induced by Water in Confinement. *Phys Rev Res* **2020**, *2* (4), 43244. https://doi.org/10.1103/PhysRevResearch.2.043244.

(8) Froltsov, V. A.; Klapp, S. H. L. Dielectric Response of Polar Liquids in Narrow Slit Pores. *J Chem Phys* **2007**, *126* (11), 114703. https://doi.org/10.1063/1.2566913.

(9) Kirkwood, J. G. The Dielectric Polarization of Polar Liquids. *J Chem Phys* **1939**, *7* (10), 911–919. https://doi.org/10.1063/1.1750343.

(10) Young, M. A.; Jayaram, B.; Beveridge, D. L. Local Dielectric Environment of B-DNA in Solution: Results from a 14 Ns Molecular Dynamics Trajectory. *J Phys Chem B* **1998**, *102* (39), 7666–7669. https://doi.org/10.1021/jp9823188.

(11) Yang, L.; Weerasinghe, S.; Smith, P. E.; Pettitt, B. M. Dielectric Response of Triplex DNA in Ionic Solution from Simulations. *Biophys J* **1995**, *69* (4), 1519–1527. https://doi.org/10.1016/S0006-3495(95)80022-6.

(12) Silvera-Batista, C. A.; Wang, R. K.; Weinberg, P.; Ziegler, K. J. Solvatochromic Shifts of Single-Walled Carbon Nanotubes in Nonpolar Microenvironments. *Physical Chemistry Chemical Physics* **2010**, *12* (26), 6990–6998. https://doi.org/10.1039/b927053a.

(13) Kruss, S.; Landry, M. P.; Vander Ende, E.; Lima, B. M. A.; Reuel, N. F.; Zhang, J.; Nelson, J.; Mu, B.; Hilmer, A.; Strano, M. Neurotransmitter Detection Using Corona Phase Molecular Recognition on Fluorescent Single-Walled Carbon Nanotube Sensors. *J Am Chem Soc* **2014**, *136* (2), 713–724. https://doi.org/10.1021/ja410433b.

(14) Kruss, S.; Salem, D. P.; Vuković, L.; Lima, B.; Vander Ende, E.; Boyden, E. S.; Strano, M. S. High-Resolution Imaging of Cellular Dopamine Efflux Using a Fluorescent Nanosensor Array. *Proceedings of the National Academy of Sciences* **2017**, *114* (8), 1789–1794. https://doi.org/10.1073/pnas.1613541114.

(15) Ackermann, J.; Metternich, J. T.; Herbertz, S.; Kruss, S. Biosensing with Fluorescent Carbon Nanotubes. *Angewandte Chemie International Edition* **2022**, *61* (18), e202112372. https://doi.org/https://doi.org/10.1002/anie.202112372.

(16) Bisker, G.; Dong, J.; Park, H. D.; Iverson, N. M.; Ahn, J.; Nelson, J. T.; Landry, M. P.; Kruss, S.; Strano, M. S. Protein-Targeted Corona Phase Molecular Recognition. *Nat Commun* **2016**, *7* (1), 10241. https://doi.org/10.1038/ncomms10241.

(17) Yadav, A.; Kelich, P.; Kallmyer, N.; Reuel, N. F.; Vuković, L. Characterizing the Interactions of Cell-Membrane-Disrupting Peptides with Lipid-Functionalized Single-Walled Carbon Nanotubes. *ACS Appl Mater Interfaces* **2023**, *15* (20), 24084–24096. https://doi.org/10.1021/acsami.3c01217.

(18) Kelich, P.; Jeong, S.; Navarro, N.; Adams, J.; Sun, X.; Zhao, H.; Landry, M. P.; Vuković, L. Discovery of DNA-Carbon Nanotube Sensors for Serotonin with Machine Learning and Near-Infrared Fluorescence Spectroscopy. *ACS Nano* **2022**, *16* (1), 736–745. https://doi.org/10.1021/acsnano.1c08271.

(19) Kim, M.; Chen, C.; Yaari, Z.; Frederiksen, R.; Randall, E.; Wollowitz, J.; Cupo, C.; Wu, X.; Shah, J.; Worroll, D.; Lagenbacher, R. E.; Goerzen, D.; Li, Y.-M.; An, H.; Wang, Y.; Heller, D. A. Nanosensor-Based Monitoring of Autophagy-Associated Lysosomal Acidification in Vivo. *Nat Chem Biol* **2023**, *19* (12), 1448–1457. https://doi.org/10.1038/s41589-023-01364-9.

(20) Antman-Passig, M.; Wong, E.; Frost, G. R.; Cupo, C.; Shah, J.; Agustinus, A.; Chen, Z.; Mancinelli, C.; Kamel, M.; Li, T.; Jonas, L. A.; Li, Y.-M.; Heller, D. A. Optical Nanosensor for Intracellular and Intracranial Detection of Amyloid-Beta. *ACS Nano* **2022**, *16* (5), 7269–7283. https://doi.org/10.1021/acsnano.2c00054.

(21) Liese, S.; Schlaich, A.; Netz, R. R. Dielectric Constant of Aqueous Solutions of Proteins and Organic Polymers from Molecular Dynamics Simulations. *J Chem Phys* **2022**, *156* (22), 224902. https://doi.org/10.1063/5.0089397.

(22) King, G.; Lee, F. S.; Warshel, A. Microscopic Simulations of Macroscopic Dielectric Constants of Solvated Proteins. *J Chem Phys* **1991**, *95* (6), 4366–4377. https://doi.org/10.1063/1.461760.

(23) Abeyrathne, C. D.; Halgamuge, M. N.; Farrell, P. M.; Skafidas, E. An Ab-Initio Computational Method to Determine Dielectric Properties of Biological Materials. *Sci Rep* **2013**, *3* (1), 1796. https://doi.org/10.1038/srep01796.

(24) Nymeyer, H.; Zhou, H.-X. A Method to Determine Dielectric Constants in Nonhomogeneous Systems: Application to Biological Membranes. *Biophys J* **2008**, *94* (4), 1185–1193. https://doi.org/10.1529/biophysj.107.117770.

(25) Smith, P. E.; Pettitt, B. M. Modeling Solvent in Biomolecular Systems. *J Phys Chem* **1994**, *98* (39), 9700–9711. https://doi.org/10.1021/j100090a002.

(26) Tanizaki, S.; Feig, M. A Generalized Born Formalism for Heterogeneous Dielectric Environments: Application to the Implicit Modeling of Biological Membranes. *J Chem Phys* **2005**, *122* (12), 124706. https://doi.org/10.1063/1.1865992.

(27) Smith, P. E.; Brunne, R. M.; Mark, A. E.; Van Gunsteren, W. F. Dielectric Properties of Trypsin Inhibitor and Lysozyme Calculated from Molecular Dynamics Simulations. *J Phys Chem* **1993**, *97* (9), 2009–2014. https://doi.org/10.1021/j100111a046.

(28) de Leeuw, S. W.; Perram, J. W.; Smith, E. R.; Rowlinson, J. S. Simulation of Electrostatic Systems in Periodic Boundary Conditions. I. Lattice Sums and Dielectric Constants. *Proceedings of the Royal Society of London. A. Mathematical and Physical Sciences* **1980**, *373* (1752), 27–56. https://doi.org/10.1098/rspa.1980.0135.

(29) Neumann, M.; Steinhauser, O.; Pawley, G. S. Consistent Calculation of the Static and Frequency-Dependent Dielectric Constant in Computer Simulations. *Mol Phys* **1984**, *52* (1), 97–113. https://doi.org/10.1080/00268978400101081.

(30) Humphrey, W.; Dalke, A.; Schulten, K. VMD: Visual Molecular Dynamics. *J Mol Graph* **1996**, *14* (1), 33–38. https://doi.org/https://doi.org/10.1016/0263-7855(96)00018-5.

(31) Phillips, J. C.; Hardy, D. J.; Maia, J. D. C.; Stone, J. E.; Ribeiro, J. V.; Bernardi, R. C.; Buch, R.; Fiorin, G.; Hénin, J.; Jiang, W.; McGreevy, R.; Melo, M. C. R.; Radak, B. K.; Skeel, R. D.; Singharoy, A.; Wang, Y.; Roux, B.; Aksimentiev, A.; Luthey-Schulten, Z.; Kalé, L. V.; Schulten, K.; Chipot, C.; Tajkhorshid, E. Scalable Molecular Dynamics on CPU and GPU Architectures with NAMD. *Journal of Chemical Physics* **2020**, *153* (4). https://doi.org/10.1063/5.0014475.

(32) Vanommeslaeghe, K.; Hatcher, E.; Acharya, C.; Kundu, S.; Zhong, S.; Shim, J.; Darian, E.; Guvench, O.; Lopes, P.; Vorobyov, I.; Mackerell, A. D. CHARMM General Force Field: A Force Field for Drug-like Molecules Compatible with the CHARMM All-Atom Additive Biological Force Fields. *J Comput Chem* **2010**, *31* (4), 671–690. https://doi.org/10.1002/jcc.21367.

(33) Huang, J.; Mackerell, A. D. CHARMM36 All-Atom Additive Protein Force Field: Validation Based on Comparison to NMR Data. *J Comput Chem* **2013**, *34* (25), 2135–2145. https://doi.org/10.1002/jcc.23354.

(34) Klauda, J. B.; Venable, R. M.; Freites, J. A.; O'Connor, J. W.; Tobias, D. J.; Mondragon-Ramirez, C.; Vorobyov, I.; MacKerell, A. D.; Pastor, R. W. Update of the CHARMM All-Atom Additive Force Field for Lipids: Validation on Six Lipid Types. *Journal of Physical Chemistry B* **2010**, *114* (23), 7830–7843. https://doi.org/10.1021/jp101759q.

(35) Darden, T.; York, D.; Pedersen, L. Particle Mesh Ewald: An N·log(N) Method for Ewald Sums in Large Systems. *J Chem Phys* **1993**, *98* (12), 10089–10092. https://doi.org/10.1063/1.464397.

(36) Bauer, P.; Hess, B.; Lindahl, E. GROMACS 2022.5 Source Code. Zenodo February 2023. https://doi.org/10.5281/zenodo.7586780.

(37) Parrinello, M.; Rahman, A. Polymorphic Transitions in Single Crystals: A New Molecular Dynamics Method. *J Appl Phys* **1981**, *52* (12), 7182–7190. https://doi.org/10.1063/1.328693.

(38) Evans, D. J.; Holian, B. L. The Nose–Hoover Thermostat. *J Chem Phys* **1985**, *83* (8), 4069–4074. https://doi.org/10.1063/1.449071.

(39) Nosé, S.; Klein, M. L. Constant Pressure Molecular Dynamics for Molecular Systems. *Mol Phys* **1983**, *50* (5), 1055–1076. https://doi.org/10.1080/00268978300102851.

(40) Hess, B.; Bekker, H.; Berendsen, H. J. C.; Fraaije, J. G. E. M. LINCS: A Linear Constraint Solver for Molecular Simulations. *J Comput Chem* **1997**, *18* (12), 1463–1472. https://doi.org/https://doi.org/10.1002/(SICI)1096-987X(199709)18:12<1463::AID-JCC4>3.0.CO;2-H.

(41) Jorgensen, W. L.; Jenson, C. Temperature Dependence of TIP3P, SPC, and TIP4P Water from NPT Monte Carlo Simulations: Seeking Temperatures of Maximum Density. *J Comput Chem* **1998**, *19* (10), 1179–1186. https://doi.org/https://doi.org/10.1002/(SICI)1096-987X(19980730)19:10<1179::AID-JCC6>3.0.CO;2-J.

(42) Meneses-Juárez, E.; Rivas-Silva, J. F.; González-Melchor, M. Static Dielectric Constant of Water within a Bilayer Using Recent Water Models: A Molecular Dynamics Study. *Journal of Physics Condensed Matter* **2018**, *30* (19). https://doi.org/10.1088/1361-648X/aab9ee.

(43) Teschke, O.; Ceotto, G.; de Souza, E. F. Interfacial Water Dielectric-Permittivity-Profile Measurements Using Atomic Force Microscopy. *Phys Rev E Stat Phys Plasmas Fluids Relat Interdiscip Topics* **2001**, *64* (1), 10. https://doi.org/10.1103/PhysRevE.64.011605.

(44) Cherepanov, D. A.; Feniouk, B. A.; Junge, W.; Mulkidjanian, A. Y. Low Dielectric Permittivity of Water at the Membrane Interface: Effect on the Energy Coupling Mechanism in Biological Membranes. *Biophys J* **2003**, *85* (2), 1307–1316. https://doi.org/10.1016/S0006-3495(03)74565-2.

(45) Hanai, T.; Haydon, D. A.; Taylor, J. Polar Group Orientation and the Electrical Properties of Lecithin Bimolecular Leaflets. *J Theor Biol* **1965**, *9* (2), 278–296. https://doi.org/https://doi.org/10.1016/0022-5193(65)90113-X.

(46) Haydon, D. A. Properties of Lipid Bilayers at a Water-Water Interface. *J Am Oil Chem Soc* **1968**, *45* (4), 230–240. https://doi.org/https://doi.org/10.1007/BF02652418.

(47) Silvera-Batista, C. A.; Wang, R. K.; Weinberg, P.; Ziegler, K. J. Solvatochromic Shifts of Single-Walled Carbon Nanotubes in Nonpolar Microenvironments. *Physical Chemistry Chemical Physics* **2010**, *12* (26), 6990–6998. https://doi.org/10.1039/b927053a.

(48) Choi, J. H.; Strano, M. S. Solvatochromism in Single-Walled Carbon Nanotubes. *Appl Phys Lett* **2007**, *90* (22), 223114. https://doi.org/10.1063/1.2745228.

(49) Antonucci, A.; Kupis-Rozmysłowicz, J.; Boghossian, A. A. Noncovalent Protein and Peptide Functionalization of Single-Walled Carbon Nanotubes for Biodelivery and Optical Sensing Applications. *ACS Applied Materials and Interfaces*. American Chemical Society April 5, 2017, pp 11321–11331. https://doi.org/10.1021/acsami.7b00810.

(50) Safaee, M. M.; Gravely, M.; Rocchio, C.; Simmeth, M.; Roxbury, D. DNA Sequence Mediates Apparent Length Distribution in Single-Walled Carbon Nanotubes. *ACS Appl Mater Interfaces* **2019**, *11* (2), 2225–2233. https://doi.org/10.1021/acsami.8b16478.

(51) Alizadehmojarad, A. A.; Zhou, X.; Beyene, A. G.; Chacon, K. E.; Sung, Y.; Pinals, R. L.; Landry, M. P.; Vuković, L. Binding Affinity and Conformational Preferences Influence Kinetic Stability of Short Oligonucleotides on Carbon Nanotubes. *Adv Mater Interfaces* **2020**, *7* (15). https://doi.org/10.1002/admi.202000353.

(52) Bisker, G.; Dong, J.; Park, H. D.; Iverson, N. M.; Ahn, J.; Nelson, J. T.; Landry, M. P.; Kruss, S.; Strano, M. S. Protein-Targeted Corona Phase Molecular Recognition. *Nat Commun* **2016**, *7*. https://doi.org/10.1038/ncomms10241.

(53) Zheng, M.; Jagota, A.; Semke, E. D.; Diner, B. A.; McLean, R. S.; Lustig, S. R.; Richardson, R. E.; Tassi, N. G. DNA-Assisted Dispersion and Separation of Carbon Nanotubes. *Nat Mater* **2003**, *2* (5), 338–342. https://doi.org/10.1038/nmat877.

(54) Qiao, R.; Ke, P. C. Lipid-Carbon Nanotube Self-Assembly in Aqueous Solution. *J Am Chem Soc* **2006**, *128* (42), 13656–13657. https://doi.org/10.1021/ja063977y.

(55) Kallmyer, N. E.; Agarwal, S.; Eeg, D.; Khor, R.; Roby, N.; Vela Ramirez, A.; Hillier, A. C.; Reuel, N. F. Lipid-Functionalized Single-Walled Carbon Nanotubes as Probes for Screening Cell Wall Disruptors. *ACS Appl Mater Interfaces* **2023**, *15* (38), 44621–44630. https://doi.org/10.1021/acsami.3c06592.

(56) Coster, H. G. L. The Physics of Cell Membranes. *J Biol Phys* **2003**, *29* (4), 363–399. https://doi.org/10.1023/A:1027362704125.

(57) Dilger, J. P.; McLaughlin, S. G. A.; McIntosh, T. J.; Simon, S. A. The Dielectric Constant of Phospholipid Bilayers and the Permeability of Membranes to Ions. *Science (1979)* **1979**, *206* (4423), 1196–1198. https://doi.org/10.1126/science.228394.

(58) Greene, D.; Qi, R.; Nguyen, R.; Qiu, T.; Luo, R. Heterogeneous Dielectric Implicit Membrane Model for the Calculation of MMPBSA Binding Free Energies. *J Chem Inf Model* **2019**, *59* (6), 3041–3056. https://doi.org/10.1021/acs.jcim.9b00363.

(59) Nymeyer, H.; Zhou, H. X. A Method to Determine Dielectric Constants in Nonhomogeneous Systems: Application to Biological Membranes. *Biophys J* **2008**, *94* (4), 1185–1193. https://doi.org/10.1529/biophysj.107.117770.

(60) Huang, W.; Levitt, D. G. Theoretical Calculation of the Dielectric Constant of a Bilayer Membrane. *Biophys J* **1977**, *17* (2), 111–128. https://doi.org/10.1016/S0006-3495(77)85630-0.

(61) Vitkova, V.; Mitkova, D.; Antonova, K.; Popkirov, G.; Dimova, R. Sucrose Solutions Alter the Electric Capacitance and Dielectric Permittivity of Lipid Bilayers. *Colloids Surf A Physicochem Eng Asp* **2018**, *557*, 51–57. https://doi.org/10.1016/j.colsurfa.2018.05.011.

(62) Gramse, G.; Dols-Perez, A.; Edwards, M. A.; Fumagalli, L.; Gomila, G. Nanoscale Measurement of the Dielectric Constant of Supported Lipid Bilayers in Aqueous Solutions with Electrostatic Force Microscopy. *Biophys J* **2013**, *104* (6), 1257–1262. https://doi.org/https://doi.org/10.1016/j.bpj.2013.02.011.

(63) Vitkova, V.; Yordanova, V.; Staneva, G.; Petkov, O.; Stoyanova-Ivanova, A.; Antonova, K.; Popkirov, G. Dielectric Properties of Phosphatidylcholine Membranes and the Effect of Sugars. *Membranes (Basel)* **2021**, *11* (11). https://doi.org/10.3390/membranes11110847.

(64) Dols-Perez, A.; Gramse, G.; Calò, A.; Gomila, G.; Fumagalli, L. Nanoscale Electric Polarizability of Ultrathin Biolayers on Insulating Substrates by Electrostatic Force Microscopy. *Nanoscale* **2015**, *7* (43), 18327–18336. https://doi.org/10.1039/C5NR04983K.

(65) Zhang, Z.; Li, Y.; Xiang, Z.; Huang, Y.; Wang, R.; Chang, C. Dielectric Dispersion Characteristics of the Phospholipid Bilayer with Subnanometer Resolution from Terahertz to Mid-Infrared. *Front Bioeng Biotechnol* **2022**, *10*. https://doi.org/10.3389/fbioe.2022.984880.

(66) Stern, H. A.; Feller, S. E. Calculation of the Dielectric Permittivity Profile for a Nonuniform System: Application to a Lipid Bilayer Simulation. *J Chem Phys* **2003**, *118* (7), 3401–3412. https://doi.org/10.1063/1.1537244.

(67) Gramse, G.; Dols-Perez, A.; Edwards, M. A.; Fumagalli, L.; Gomila, G. Nanoscale Measurement of the Dielectric Constant of Supported Lipid Bilayers in Aqueous Solutions with Electrostatic Force Microscopy. *Biophys J* **2013**, *104* (6), 1257–1262. https://doi.org/10.1016/j.bpj.2013.02.011.

(68) Nymeyer, H.; Zhou, H. X. A Method to Determine Dielectric Constants in Nonhomogeneous Systems: Application to Biological Membranes. *Biophys J* **2008**, *94* (4), 1185–1193. https://doi.org/10.1529/biophysj.107.117770.

(69) Simonson, T. Accurate Calculation of the Dielectric Constant of Water from Simulations of a Microscopic Droplet in Vacuum. *Chem Phys Lett* **1996**, *250* (5), 450–454. https://doi.org/https://doi.org/10.1016/0009-2614(96)00058-9.